ELSEVIER

Contents lists available at ScienceDirect

Journal of Inorganic Biochemistry

journal homepage: www.elsevier.com/locate/jinorgbio





Recent advances in the preclinical development of responsive MRI contrast agents capable of detecting hydrogen peroxide

Sana Karbalaei, Christian R. Goldsmith

Department of Chemistry and Biochemistry, Auburn University, Auburn, AL 36849, USA

ARTICLE INFO

Keywords:
Magnetic resonance imaging
Sensors
Redox
Redox-activated ligands
Transition metals
Lanthanides

ABSTRACT

In this review, we focus on the preclinical development and study of coordination complexes that act as magnetic resonance imaging (MRI) contrast agent sensors for hydrogen peroxide. Redox-responsive probes have been developed that provide signals that can be detected through traditional T_1 -weighted 1 H, 19 F, and Chemical Exchange Saturation Transfer MRI. The sensors can also be classified with respect to whether the change in the signal corresponds to the oxidation of the metal ion or the organic ligand.

1. Introduction

1.1. Reactive Oxygen Species (ROS) in biology

Reactive oxygen species (ROS), including hydrogen peroxide (H_2O_2) , superoxide anion radical (O_2^-) , and hydroxyl radical (OH), are produced in small quantities during many physiological processes. In eukaryotic cells, it is estimated that over 90% of ROS are generated by the mitochondria when electrons inadvertently escape from the mitochondrial electron-transport chain [1–3]. The cell uses a variety of antioxidants, such as superoxide dismutase and catalase enzymes, in order to regulate ROS levels [4–7].

Although ROS have been demonstrated to serve essential and beneficial roles in several biological processes, such as cellular signaling [8–11] and the modulation of neuron and cardiomyocyte excitability [12–17], high concentrations of these oxidants are harmful and lead to organ-damaging oxidative stress through the degradation of biomolecules such as proteins and lipids. The overproduction of ROS has been linked to many and diverse health conditions that include a variety of inflammatory [18,19], cardiovascular [20–24], and neurological disorders [25–29]. The roles of ROS in disease progression, however, have not been fully resolved and require further elucidation. Methods that can monitor ROS concentrations in biological environments have the potential to directly address this issue. Appropriate sensors for ROS could enable the earlier diagnoses of these health conditions by linking spatiotemporal patterns of oxidative stress to specific disorders. Further,

probes capable of detecting ROS could also direct researchers to more effective treatments for these conditions by providing more information about their underlying physiological bases.

1.2. H_2O_2 detection – general considerations for sensor design

Although there are many sorts of ROS, this article will focus on sensors that can detect $\rm H_2O_2$. ROS are intrinsically highly reactive [30,31], and the cell produces a variety of antioxidants designed to lower their numbers even further. Consequently, each of these species accumulates at relatively low levels. Although such numbers have not yet been firmly defined, the steady-state *in vivo* concentrations of $\rm H_2O_2$ and $\rm O_2^-$ in a typical cell are estimated to be 0.1 μM and 0.1 nM, respectively [32]. OH and OOH radicals are too reactive to be reliably intercepted by an antioxidant or sensor, and their steady-state levels would be even lower. Of the ROS listed in this paragraph, $\rm H_2O_2$ is arguably the easiest analyte to pursue due to its higher abundance.

In designing a practical sensor, one must worry about the selectivity of its response. Different analytes may react with a probe to yield similar species with similar or even identical spectroscopic signatures; in such circumstances, one cannot distinguish these analytes. Ideally, a ROS sensor will be able to differentiate one ROS from another. In practice, this is difficult to achieve since different oxidants, including O_2 , can enable the same chemical transformation that produces the signal. Possible reactivity with O_2 is arguably the greater concern since a probe that non-discriminately reacts with ROS nonetheless detects oxidative

E-mail address: crgoldsmith@auburn.edu (C.R. Goldsmith).

^{*} Corresponding author.

stress of some sort. Ideally, the redox potential of the sensor is such that it can be oxidized by one or more ROS, but not by O_2 . Many of the sensors described in this review will react with O_2 ; some are included in the discussion since this side reactivity is often either slight enough to ignore over a short period of time or occurs much more slowly than the reaction with H_2O_2 . In other cases, we discuss O_2 -responsive contrast agents that do not have a documented response to H_2O_2 in order to introduce a strategy that could be applied to H_2O_2 sensing.

Even in situations where the sensor is not sensitive to O_2 and reacts specifically with one ROS, it can be difficult to attribute a probe's response to just a single ROS since these species can chemically transform into each other under physiological conditions. Whenever it is in a protic environment, O_2 ", for instance, reacts with itself to yield O_2 and H_2O_2 . A compound that is activated by H_2O_2 in water can therefore also be activated either directly or indirectly by O_2 ". H_2O_2 reacts with transition metals to form $\cdot OH$ and $\cdot OOH$, which are both extremely potent oxidants that will certainly activate sensors designed to react with either O_2 or H_2O_2 [33,34].

Magnetic resonance imaging (MRI)-based sensors are typically administered above 10 µM in order to provide signal-to-noise ratios that are high enough to unambiguously detect their analytes [35-47]. With T_1 -weighted MRI contrast agents, this 10 μ M value is very much a lower limit. These are frequently formulated at concentrations closer to 0.5 M and administered to provide 10s or 100s of µmol of contrast agent per kg of body weight. The sensor concentrations are therefore much higher than physiological ROS levels. ROS sensors need to be activated by small but continually replenishing pools of oxidants. The reactions that activate the redox-sensitive compounds described in this review consume the ROS but can sometimes be reversed by reductants, including many that are physiologically produced. Consequently, some of the described sensors can potentially revert to their pre-activated states upon the alleviation of the oxidative stress. Given the low steady-state concentrations of ROS, it may take a prolonged period of time for a MRI-based sensor to reach equilibrium.

Generally, sensors can be classified into two major categories: turnon and turn-off. In the former case, the signal increases upon activation. A turn-on fluorescent compound, for instance, may become brighter or emit light at a new wavelength. In a turn-off sensor, the signal decreases or disappears entirely upon reaction with the analyte; the system more closely resembles what would be observed in the absence of the sensor. With T_1 -weighted contrast agents, a turn-off response will reduce the relaxivity and lessen its ability to sharpen image contrast. Turn-on sensors tend to be more practical since a diminished signal can result from a variety of different scenarios, including decomposition of the probe or its diffusion out of the area of study. Ratiometric probes provide distinct signals in their pre-activated and activated states; these are attractive in that they can more readily allow researchers to determine the extent of sensor activation in a specific region. Many of the contrast agent ROS probes with 19F MRI outputs described in this review are ratiometric sensors as are the compounds with multiple modalities.

1.3. Why MRI?

MRI has been used extensively for the non-invasive visualization of soft tissues within whole-body subjects. In addition to identifying and outlining morphological features, MRI can potentially provide insight into biochemical processes within these tissues through the use of a chemically responsive contrast agent [37,48]. A chemical probe that produces a change to the MR image upon oxidation by an ROS could be used to non-invasively monitor biological redox environments using clinically approved MRI scanners.

This article is heavily indebted to a number of other reviews of redox-responsive MRI contrast agents [48–54]. The focus of this review will be on coordination complex probes that have been documented to react with $\rm H_2O_2$. Compounds that react with reductants or have only had their response with $\rm O_2$ characterized will generally not be discussed at length

unless they illustrate concepts that have been or could readily be applied to the detection of H_2O_2 . As will be detailed in the final section of this review, H_2O_2 probes will need to traverse a complicated path to the clinic. An excellent *in vitro* response to H_2O_2 does not necessary lead to an adequate *in vivo* response, and the pharmacological properties of the sensor (e.g. toxicity, clearance from the body) need to be thoroughly assessed before one can even consider using these probes for clinical diagnoses. This article will primarily focus on the preclinical development of these sensors but will nonetheless highlight instances where complexes have been used to image oxidative activity in biological samples.

2. Fundamental MRI theory

MRI instruments apply a static magnetic field and specific radio-frequency (RF) pulses. Under the magnetic field, the nuclei with non-zero spin precess at the Larmor frequency (ω), determined by the field strength (B0) and the gyro-magnetic ratio (γ) of the nucleus under investigation (Eq. 1).

$$\omega = \gamma \bullet B0 \tag{1}$$

The RF pulses, matched to the Larmor frequency, cause the nuclei spins to rotate or 'tip' out of alignment from the static magnetic field by angle (α) determined by RF pulse strength (B1) and pulse duration (τ).

$$\alpha = \tau \bullet B1 \tag{2}$$

After the pulse, the tipped spins continue to precess and radiate a secondary echo RF signal. The MRI scanner detects the echo signals released by the relaxing nuclei over time as the spins revert to their original magnetization equilibrium and converts these data into an image. Most frequently, ¹H nuclei are visualized, but other nuclei, such as ¹⁹F, have also been explored as reporters [49]. Since water is the major source of ¹H nuclei within the body, ¹H-based MRI usually differentiates soft tissues from each other based on their water content, with the more water-rich regions being more readily visualized.

Both the relaxation times of magnetically resonant nuclei and their concentrations impact the contrast of the MR image. Endogenous contrast is not always sufficient to delineate abnormalities and differentiate nearby tissues with similar water contents, but this problem can sometimes be resolved by the administration of contrast agents, which most frequently work by shortening the relaxation time of the visualized nuclei [49,55–57]. There are two relaxation pathways: longitudinal relaxation T_1 (spin-lattice relaxation) and transverse relaxation T_2 (spin-spin relaxation). T_1 and T_2 are both time constants; the corresponding rates of nuclear relaxation are associated with the rate constants $1/T_1$ and $1/T_2$.

All of the ROS-responsive MRI contrast agents described in this review rely on one or two of three fundamental physical processes to alter the MR image: T_1 -weighted 1 H relaxation, 19 F relaxation, and chemical exchange saturation transfer (CEST).

2.1. T₁-weighted relaxation

The most widely employed MRI contrast agents use highly paramagnetic metal ions to hasten the rate of T_I -associated relaxation for the 1 H nuclei of nearby water molecules. This improves the T_I -weighted (T_{Iw}) contrast of the signal. Although a wide array of mononuclear Gd (III), Fe(III), and Mn(II) complexes have been demonstrated to act as MRI contrast agents [35–40,55,58,59,61–69], only a handful of Gd(III) complexes are currently approved for clinical use [49].

The longitudinal proton relaxivity (r_1) of a compound is the primary measure of its effectiveness as a T_1 relaxation agent. Higher values of r_1 result in stronger contrast. The r_1 is related to the observed T_1 $(T_{1,obs})$ through the following relationship:

$$\frac{1}{T_{\text{Lobs}}} = \frac{1}{T_{\text{Ldia}}} + r_1 C \tag{3}$$

In Eq. 3, $T_{1,dia}$ is the longitudinal relaxation time in the absence of the contrast agent, and C is the concentration of the contrast agent.

The r_1 value is determined by the nature of the interactions between the contrast agent and molecules from the bulk water. The inner-sphere component (r_{IIS}) originates from the interactions between the electron spin of the paramagnetic metal center and the nuclear spins from protons of water molecules that are directly coordinated to the metal ion. The outer-sphere component to the relaxivity (r_{1OS}) results from interactions with nearby non-coordinated water molecules. The secondsphere component (r_{155}) results from the electron spin of the metal ion interacting with water molecules that are hydrogen bonding to the metal complex. Of the three contributors to r_1 , the r_{US} is the most straightforward to manipulate through synthetic modifications to the contrast agent. The inner-sphere relaxation is dependent on the aquation number of metal center (q), the relaxation time (T_{1m}) , and the mean residency time (τ_m) of the coordinated water molecules (Eq. 4) [55]. The magnitude of inner-sphere relaxation can be modified by changing the structure of ligand. A less highly coordinating polydentate ligand, for instance, will leave more open coordination sites for water, increasing q. One must be cautious in making such modifications, however, since the polydentate ligand needs to coordinate tightly enough to the metal ion to keep the contrast agent intact in water. Altering the charge of the donor atoms will impact the rate of the water exchange and thereby $\tau_{\rm m}$. The metal ion strongly influences T_{1m} , with more paramagnetic ions leading to shorter values and higher r_{1IS} .

$$r_{\text{LIS}} = \frac{q/[\text{H2O}]}{T \text{I} m + \tau \text{m}} \tag{4}$$

The relaxation time of the water molecules coordinated to the metal center (T_{1m}) can also be modified by altering the correlation time (τ_c) , which is defined the time needed for 1 rad rotation perpendicular to the applied field. τ_c depends on three dynamic processes (Eq. 5): the residency time (τ_m) , the field-dependent electronic longitudinal relaxation time (T1e), and the rotational correlation time of the metal compound (τ_R) [70]. The fastest dynamic process contributes the most to τ_c . For most Gd(III) and Mn(II) complexes, T1e and τ_m are on the ns timescale, whereas τ_R is on the ps time scale. Consequently, τ_c is approximately equal to τ_R for these complexes.

$$\frac{1}{\tau_c} = \frac{1}{\tau_R} + \frac{1}{\tau_m} + \frac{1}{T_{l_e}} \tag{5}$$

The rotational correlation time can be slowed by binding the contrast agent to a biomacromolecule through either a non-covalent or covalent linkage. The impact of tethering the contrast agent to a larger structure on the r_I is highly dependent on the magnetic field strength. Larger gains to the r_I are generally seen with weaker fields [71,72].

2.2. 19F MRI

The physical basis of ^{19}F MRI is similar to that of ^{1}H MRI, and the two nuclei can be imaged with mostly the same instrumentation [73–75]. ^{19}F MRI data can be acquired on a traditional ^{1}H MRI scanner equipped with a specialized radiofrequency coil. The primary difference between these two forms of MRI is that the longitudinal (R_{1}) and transverse (R_{2}) rates of relaxation for ^{19}F are more similar to each other, and one cannot effectively weight the measurements towards one process as is frequently done with ^{1}H MRI. The signal intensity (I) is approximated by Eq. 6, where N(F) is the density of ^{19}F nuclei and T_{R} and T_{E} are the repetition and echo times of the pulse sequence. The strongest signals will result when T_{1} and T_{2} are approximately equal.

$$I = N(F) exp.(-T_E/T_2)[1-2 exp.(-(T_R-T_E/2)/T_1) + exp.(-T_E/T_1)]$$
 (6)

 $^{19}\mathrm{F}$ MRI has two significant advantages over $T_{I}\text{-}\text{weighted}$ $^{1}\mathrm{H}$ MRI. First, there is essentially no background signal from physiological fluorine sources since the small amount of fluorine that is present in the body is embedded into the solid matrices of the teeth and bones. The inability of these matrices to tumble increases R_{2} , leading to extreme line broadening and the effective loss of the $^{19}\mathrm{F}$ MRI signal. Second, the chemical shifts of $^{19}\mathrm{F}$ nuclei are spread over a 300 ppm range, facilitating the differentiation of fluorine-containing species. Consequently, if the $^{19}\mathrm{F}$ signals of the pre-activated and activated forms of a sensor have sufficiently different energies, a fluorine-containing probe could provide a ratiometric response, even without a secondary spectroscopic output.

The chief disadvantage to ¹⁹F MRI is that successful imaging often requires lengthy acquisition times and/or high loadings of the contrast agent. The low sensitivity results from two factors. First, there are few imageable ¹⁹F nuclei in a typical experiment, and the visualizable ¹⁹F comes almost exclusively from an added contrast agent. With T_1 weighted ¹H MRI, conversely, the signal originates from the bulk water molecules. The low numbers of ¹⁹F nuclei typically lead to poor signalto-noise ratios. The signal quality can be improved by installing multiple chemically equivalent F atoms onto the imaging agent. Unfortunately, this can introduce another problem: heavily fluorinated molecules tend to be poorly soluble in water [76]. Second, the T_1 relaxation times of 19 F nuclei tend to be long; a typical value for a diamagnetic molecule is about 0.5–3 s. The T_1 can be shortened by using a paramagnetic molecule as the fluorine source. As with ¹H MRI, more paramagnetic species tend to shorten T_1 to greater extents. However, these ions can also shorten T_2 , which leads to line broadening [75]. Mn(II), which is effective in increasing the contrast of T_{1w} ¹H MRI, severely attenuates 19 F MRI signals due to its tendency to decrease T_2 [75,77].

2.3. Chemical Exchange Saturation Transfer (CEST)

MRI-visualizable nuclei can potentially exchange between multiple chemical species, with the nucleus having a discrete resonance frequency for each chemical environment. Saturating one of these frequencies with the appropriate radiation will decrease the intensity of the signals associated with the other chemical environments. This phenomenon is referred to as Chemical Exchange Saturation Transfer (CEST) [78]. Compounds with N—H or O—H bonds, for instance, can exchange ¹H protons with those from water molecules. Irradiating at the resonance frequencies of the N—H or O—H protons will weaken the signal arising from the water nuclei [79]. Reducing the intensity of the total water signal results in decreased contrast for the MR image [52,79]. As such, CEST is intrinsically a turn-off phenomenon, but a turn-on sensor could be created if one were to start with a CEST-active compound that converts to a CEST-inactive species upon reaction with an analyte.

CEST is more efficient when the ¹H nuclei exchange between chemical environments with greatly different resonance frequencies [52,79]. With diamagnetic CEST agents, there tends to be strong overlap between the contrast agent's resonance frequencies and that of the bulk water. Although only certain paramagnetic metal ions, such as Gd(III) and Mn(II), relax hydrogen nuclei quickly enough to allow T_I -weighted MRI contrast enhancement, most paramagnetic metal ions shift the hyperfine resonance energies of nearby nuclei to extents that dwarf those attainable with diamagnetic species [52]. CEST with paramagnetic agents is often referred to as PARACEST. Traditional MRI contrast agents rely upon rapid water molecule exchange into the coordination sphere of the paramagnetic ion to enhance the MRI contrast [55]. Such rapid water molecule exchange essentially nullifies CEST by coalescing the frequencies associated with the different chemical environments associated with the nuclei into a single signal.

One disadvantage to using CEST for ROS sensing is that the CEST effect is highly sensitive to pH and temperature; it can therefore be difficult to attribute a change in the local CEST signal to just a change in the redox environment. The local pH and temperature impact both the resonance frequencies of the exchanging nuclei and the rate of exchange. Another significant disadvantage is that the RF pulses needed for CEST are much longer ($\sim 1~\rm s$) than those used for other forms of MRI ($\sim 10~\rm ms)$ [80]. These longer pulses transfer more power to the sample, potentially heating it to hazardous levels. Variations of CEST that use a series of short pulses instead of one long RF pulse are currently being explored.

3. Recently reported MRI contrast agent sensors for ROS

3.1. T₁-weighted MRI contrast agent sensors

3.1.1. Sensors that rely on a change to the oxidation state of the metal ion Although the complex in question was not explicitly demonstrated to react with H2O2, a sensor reported by Aime et al. in 2000 deserves mention for using a Mn(III/II) couple to detect O2 [35]. The authors' early use of a metal-based redox couple to detect an oxidant in conjunction with MRI has unquestionably influenced the other work in this section. Nuclear magnetic resonance dispersion data indicated that the r_1 values of the Mn(II) and Mn(III) complexes with the porphyrinic ligand TPPS⁸⁻ (Scheme 1) were too similar above \sim 3 MHz to distinguish by MRI. Aime et al., however, were able to better separate the relaxivities of these compounds at higher fields by encapsulating them into cyclodextrin (CD) hosts. This strategy works since the r_1 of the Mn(II) species is more strongly impacted by the rotational motion and $\tau_{\rm R}$; the relaxivity of the Mn(III) complex, conversely, is more dependent on the electronic relaxation time [81,82]. With a 20 MHz field, the macromolecular adducts of the Mn(II) and Mn(III) complexes with a poly-β-CD had r_1 values of 40.8 mM⁻¹ s⁻¹ and 15.2 mM⁻¹ s⁻¹, respectively [35]. Upon reaction with 40 Torr of O2, the Mn(II) complex completely converts to the Mn(III) in under 5 min. Although the addition of H₂O₂ would likely result in a similar, if not identical, turn-off in r_1 , the speed of the O₂ oxidation would prevent the Mn(II)-TPPS⁸⁻ complex from differentiating the two oxidants.

Manganese complexes with porphyrinic ligands could potentially be used to detect H_2O_2 if the O_2 reactivity were significantly slowed. Pinto et al. reported a manganese-containing O_2 sensor with a porphyrin ligand covalently modified with polyethylene glycol (PEG) groups (Scheme 2) [83]. Much like the aforementioned TPPS⁸⁻/CD system, the Mn(II) complex displays a much higher r_I than the Mn(III), but without the necessity of including a second component to make a macromolecular adduct. The Mn(III) can be rapidly reduced to the Mn(II) using

Scheme 1. Structure of the 5,10,15,20-tetrakis-(*p*-sulfonatophenyl)porphinate (TPPS⁸-) ligand used in reference [35].

Scheme 2. Structure of 5,10,15,20-(4-PEG500–2,3,5,6-fluorophenyl) porphyrin, the PEG-derivatized ligand used in reference [83].

ascorbic acid or β -mercaptoethanol. Notably, the authors describe the oxidation of the Mn(II) form by O_2 , as being "quite slow but... fully achieved after 24 h." [83] Although the complex could potentially react with H_2O_2 quickly enough to selectively detect it over O_2 , the oxidation of the Mn(II) form by H_2O_2 was not described.

The research groups led by Caravan and Gale have developed a series of responsive MRI contrast agents that rely on M(III/II) redox processes to detect biologically relevant reductants and oxidants, including $\rm H_2O_2$ [84–87]. Much of the T_1 response results from the change to the paramagnetism of the metal center, with the more paramagnetic species in the redox couple having a shorter T_{1m} . The aquation number, q, also impacts the r_1 , but this can only be reliably measured for Mn(II) [88]. q would be anticipated to decrease upon oxidation due to the smaller size of the oxidized metal ion; this would reduce r_1 as a consequence. Most of the contrast agents reported by Caravan, Gale, and co-workers contain manganese and display analogous turn-off responses to H_2O_2 [84–86], but a more recent sensor contains iron and converts to a species with a higher relaxivity upon exposure to H_2O_2 [87].

In the manganese-containing contrast agents initially reported by Loving et al., the metal ions are coordinated to derivatives of ethylenediaminetetraacetate (EDTA $^4-$, Scheme 3) [84]. [Mn $^{II}(\text{EDTA})$ (H $_2\text{O})]^{2-}$ itself is difficult to oxidize. The Mn(II) complex with EDTA $^4-$ is straightforward to isolate and characterize, does not react with air in water [89–91], and has an irreversible oxidation feature with a Mn(III/II) reduction potential of 633 mV vs. NHE [84]. Replacing the carboxylate groups of the EDTA $^4-$ with phenolates yields ligands that stabilize Mn(III) to a greater extent. Although the diphenolate ligand HBED $^4-$ does not form a stable Mn(II) complex [92], the derivative with just a single phenolate group (HBET $^4-$) adequately stabilizes both the +2 and +3 oxidation states [84].

The Mn(II) and Mn(III) complexes with HBET can therefore react with oxidants and reductants, respectively [84]. Glutathione (GSH) reduces the Mn(III) compound to Mn(II), with a concomitant increase in r_1 (Table 1). When the Mn(III) is reduced by 1 mM GSH, a concentration that represents the lower limit for cellular glutathione [93], the half-life of the reaction is approximately 30 min. The Mn(II) form of the contrast agent can be oxidized back to the Mn(III) with H_2O_2 with a turn-off response in r_1 . With 1 mM H_2O_2 , 70% of the Mn(II) gets re-oxidized to Mn(III) in 4 min. The authors were concerned about the *in vivo* stability of the probe, noting that EDTA⁴⁻ readily removes the manganese [84].

With manganese complexes, water stability is a major concern. Coordination complexes with Mn(II) tend to be less stable than analogous species with other transition metal ions [94]. Physiologically relevant

Scheme 3. Structures of ligands for the manganese complexes discussed in references [84–86]. $EDTA^{4-}=$ ethylenediamine-N,N'-tetraacetate; $HBET^{4-}=N$ -(phenolate)ethylenediamine-N,N'-triacetate; $HBED^{4-}=N$,N'-bis((pyridin-2-ylmethylene)phenolate)ethylenediamine-N,N'-diacetate; N-diacetate; N-di

Table 1 Relaxivities of T_1 -weighted MRI contrast agents that respond to ROS through changes in the oxidation state of the metal ion.

| Contrast agent | $r_1 (M^{2+})$ (mM ⁻¹ s ⁻¹) | $r_1 (M^{3+})$ $(mM^{-1} s^{-1})$ | $r_1 (M^{3+})/r_1 (M^{2+})$ | Reference |
|--|---|--------------------------------------|-----------------------------|-----------|
| [Mn ^{II/III} (HBET)] ^{2-/-} | 2.76 | 1.05 | 0.38 | [84] |
| [Mn ^{II/III} (HBET- OMe)] ^{2-/-} | 3.1 | N.A. | N.A. | [85] |
| [Mn ^{II/III} (HBET- NO ₂)] ^{2-/-} | 2.3 | 0.5 | 0.22 | [85] |
| [Mn ^{II/} ^{III} (CyHBET)] ^{2-/-} | 3.3 | 0.4 | 0.12 | [85] |
| [Mn ^{II/III} (CyHBET- OMe)] ^{2-/-} | 3.3 | N.A. | N.A. | [85] |
| [Mn ^{II/III} (CyHBET- NO ₂)] ^{2-/-} | 2.3 | 0.5 | 0.22 | [85] |
| $[Mn^{II/III}(JED)]^{2-/-}$ | 3.3 | 0.5 | 0.15 | [86] |
| $[Fe^{II/III}(PyC3A)]^{-/0}$ | 0.18 | 1.8 | 10 | [87] |
| [Mn ^{II/} ^{III} (HTFBED)] ^{2-/1a} | 2.7 | 0.7 | 0.26 | [95] |

All measurements taken in pH 7.4 Tris buffer at 37 $^{\circ}\text{C}$ with a 1.4 T field unless stated otherwise.

metal chelators further complicate the issue *in vivo* as they can potentially remove metal ions from contrast agents that are ostensibly waterstable. Consequently, one major initiative within this sub-field is to stabilize the sensors to as great an extent as possible.

Gale et al. subsequently modified the HBET⁴⁻ framework by replacing the ethylene linkage between the amines with a cyclohexane to yield the CyHBET⁴⁻ series of ligands and by introducing different substituents (R = H, OMe, NO₂) onto the 5-position of the phenolate group (Scheme 3) [85]. Mn(II) and Mn(III) complexes were prepared for most of the ligands; the Mn(III) complexes with the two methoxy-derivatized ligands appear to spontaneously decompose over the course of minutes and were not successfully isolated and characterized.

The manganese compounds with the other ligands act as redox-responsive MRI contrast agents. The introduction of the cyclohexane ring modestly improves the water stabilities of the Mn(II) complexes and boosts the r_I response observed upon reduction from 2.6-fold (HBET⁴⁻) to 8.25-fold (CyHBET⁴⁻) when R = H. This benefit does not extend to the

 NO_2 -derivatized Mn(III) complexes, which display identical within error 4.6-fold r_1 enhancements upon reduction (Table 1). The addition of the nitro group decreases the r_1 of the Mn(II) complexes at pH 7.4 but does not do so consistently with the Mn(III) species – a noticeable drop is seen for the HBET^{4–} framework but not the CyHBET^{4–} (Table 1). T_2 -weighted relaxivities (r_2) were also measured and found to likewise increase upon reduction of the metal center.

The electronically modified complexes were analyzed using cyclic voltammetry. The Mn(III/II) reduction potentials fall within a narrow range, with $E_{1/2}$ varying from 0.45 to 0.57 V ν s. NHE [85]. As anticipated, the reduction potentials are highest when R = NO₂. Consequently, all of the isolated Mn(III) complexes can be reduced by L-cysteine. The nitrosylated ligands accelerate this reactivity by approximately one order of magnitude over the Mn(III) complexes with the two R = H ligands. The oxidation of the Mn(III) complexes was not studied in the 2014 report [85]. The Mn(III) complexes with the HBET-derived ligands would be anticipated to rapidly reduce to Mn(II) species in blood plasma, limiting their practical use.

Gale et al. subsequently prepared the "Janus chelator" JED^{4–} (Scheme 3), which was designed to provide differing coordination modes for Mn(II) and Mn(III) in order to improve the aqueous stabilities of both forms [86]. With this ligand, the pyridine rings were anticipated to bind to Mn(II), but not Mn(III). The phenolates, conversely, are expected to ligate Mn(III), but not Mn(III). Spectrophotometric pH titrations were used to investigate the coordination of the phenolates and confirmed that they bind to Mn(III) but not Mn(II). The JED^{4–} ligand successfully stabilizes both the Mn(II) and Mn(III) complexes, with high performance liquid chromatography traces demonstrating that more than 95% of the Mn(II) and Mn(III) compounds remain intact after 24 h in plasma. There was "little interconversion" between the two oxidation states, suggesting negligible O₂ reactivity and/or disproportionation of Mn(III).

As with the HBET⁴⁻ complex, the manganese complex with JED⁴⁻ can interconvert between Mn(II) and Mn(III) forms. The Mn(III) species can be reduced to Mn(II) by L-cysteine. In buffered water, this reduction is associated with a 6.6-fold enhancement in r_1 (Table 1). In plasma, the sensor performs more effectively, with the relaxivity increasing by a factor of 8.5. When the contrast agent is exposed to 5 equiv. of the thiol, the Mn(III) is reduced within seconds. The oxidation of [Mn^{II}(HBET)]²⁻, conversely, does not occur as readily. H₂O₂ by itself will not oxidize the

^a Measurements taken in pH 7.4 4-(2-hydroxyethyl)-1-piper-azineethanesulfonic acid (HEPES) buffer with a 0.5 T field.

Mn(II) form, but incubating the Mn(II) complex with both H_2O_2 and peroxidase rapidly oxidizes it to the Mn(III) form with the anticipated decrease in r_1 .

Most recently, Wang et al. reported a T_1 -weighted MRI contrast agent sensor that uses iron rather than manganese as the paramagnetic reporter [87]. The selection of the Fe(III/II) couple significantly impacts the r_1 response since it is the higher oxidation state that is more paramagnetic. Further and more importantly, high-spin Fe(II) complexes undergo much faster electron spin relaxation than Fe(III); this substantially decreases τ_c (Eq. 5) and thereby $1/T_1$ [96]. Even when high-spin, Fe(II) complexes are inefficient T_1 -weighted MRI contrast agents. The key advantage to this design is that the pre-activated sensor has a negligible impact on the MR image; any contrast enhancement can be largely attributed to the oxidation of the Fe(II) complex rather than the accumulation of a large amount of the pre-activated ferrous probe in an area of interest.

Although the PyC3A³⁻ ligand (Scheme 4) was found to stabilize complexes with both Fe(II) and Fe(III), the ferrous species oxidizes upon hours-long exposure to air [87]. Ascorbic acid was added to stock solutions of the Fe(II) complex to prevent premature oxidation. Based on variable pH relaxivity measurements and ¹⁷O NMR measurements with ¹⁷O-labeled water, Wang et al. concluded that the Fe(III) complex is aquated, and the NMR data indicate a fast enough rate of water exchange to support the efficient T_1 relaxation of bulk water. As with the previous Mn(III) complexes from the Caravan and Gale groups, the Fe (III) complex with PyC3A³⁻ is rapidly reduced by L-cysteine to the nearly MRI-silent Fe(II) species. Conversely, the ferrous form is readily oxidized by H₂O₂ to the higher relaxivity ferric compound. The iron system thereby displays a strong turn-on response to H₂O₂. Upon oxidation, the r_1 improves by a factor of 10 with a 1.4 T field (Table 1), and even larger percentile gains to the relaxivity are observed at 4.7 T (13.3-fold) and 11.7 T (14.5-fold). The key drawback is that the 1.8 $\mathrm{mM}^{-1} \mathrm{s}^{-1} r_1$ of the Fe(III) form is low relative to the 3–4 $\mathrm{mM}^{-1} \mathrm{s}^{-1}$ values observed for typical Mn(II)- and Gd(III)-containing MRI contrast agents; this may necessitate the administration of a higher dose of the sensor for many biological imaging applications.

The utility of the $[\mathrm{Fe^{II}}(\mathrm{PyC3A})]^-$ complex was demonstrated in an animal model of inflammation [97]. Wang et al. induced pancreatic inflammation in mice using intraperitoneal injections of caerulein and then imaged the animals before and after the administration of the contrast agent; the administered dose of the Fe(II) probe was 0.2 mmol/kg [87]. The Fe(II) complex failed to activate in the control mice but enhanced the MR image of the pancreas of animals that had been dosed with caerulein. The 1.6 mM $^{-1}$ s $^{-1}$ difference in r_I (measured in HEPES buffer) was sufficient to enable the complex to detect biologically relevant oxidative stress.

O'Neill et al. described a redox-responsive T_I -weighted MRI contrast agent that instead made use of a Co(III/II) couple [98]. The authors initially prepared a Co(III) complex with the TPA ligand (Scheme 5), $[\text{Co}^{\text{III}}(\text{TPA})(\text{acac})]^{2+}$ (acac⁻ = acetylacetonate), and determined that they were able to reduce it to a discrete Co(II) species upon reduction by

Scheme 4. Structure of the iron-binding ligand *N*-picolyl-N,N',N'-trans-1,2-cyclohexylenediaminetriacetate (PyC3A³⁻) used in reference [87].

dithionite. The complex oxidizes back to the Co(III) form upon exposure to air over the course of a few hours. The oxidation of the Co(II) by $\rm H_2O_2$ was not investigated. The Co(II) form was found to have a r_1 of approximately 0.06 mM $^{-1}$ s $^{-1}$ and a r_2 of approximately 0.24 mM $^{-1}$ s $^{-1}$ at 37 °C in pH 7.4 Tris buffer with a field strength of 9.4 T. The low r_1 value was attributed to the short electronic relaxation time of Co(II). The authors later installed carboxylate groups on the pyridine rings of TPA; the r_1 values of the resultant Co(II) complexes were approximately the same [99]. These complexes were used to successfully image the hypoxic regions of tumor spheroids, but the tumors needed to be incubated with 2 mM solutions of the Co(III) complexes for 24 h for enough of the compounds to enter the spheroids to make these visible.

Another redox-couple that has been explored for T_I -weighted MRI is Eu(III/II). Like Gd(III), Eu(II) has seven unpaired electrons in its ground state, and its complexes exhibit similarly high r_I values [100–105]. The more oxidatively stable Eu(III) complexes, conversely, have little impact on T_I but can be visualized using CEST, with a fluorinated derivative also displaying an oxidation-triggered ¹⁹F MRI response [101,102,105]. Since these latter two modes provide a turn-on signal rather than the turn-off in r_I accompanying the oxidation of Eu(II) to Eu(III), these complexes will be more fully described in the CEST portion of this review.

3.1.2. Sensors that rely on a change to the oxidation state of the organic ligand

Other T_I -weighted sensors for ROS display changes in r_I that result from oxidation of the organic ligand, rather than the metal center. Early examples include a variety of Gd(III) compounds [18,71,72,106,107]. Since Gd(III) is almost completely redox-inactive [108], the only way for a Gd(III) complex to undergo a chemical reaction with an ROS is for the organic portion of the compound to be oxidized rather than the metal.

The Chen and Bogdanov groups prepared a series of Gd(III) complexes with ligands containing pendent phenol derivatives, such as 5-hydroxytryptamine (serotonin, Scheme 6), that oligomerize upon reaction with H₂O₂ and peroxidase enzymes [18,71,72,106,107]. Unlike most of the H₂O₂ sensors described in this review, the Gd(III) complexes do not react with H₂O₂ directly; the MRI response strictly requires both the enzyme and H₂O₂. The peroxidase enzymes are needed to react with H₂O₂ and convert it to a more reactive ROS that is capable of directly activating the ligand. Myeloperoxidase (MPO), for instance, reacts with H₂O₂ and Cl⁻ to form HOCl [71]. The HOCl generated by MPO then abstracts a H atom from the phenolic portion of the ligand to generate a phenoxyl radical, which subsequently oxidatively couples to other phenolic species (Scheme 7). In the absence of other phenol-containing biomolecules, such as proteins with exposed tyrosine residues, the sensor oligomerizes [107]. The larger size of the now polynuclear Gd (III) complex slows the rotation of the paramagnetic products, increasing τ_R and thereby r_1 .

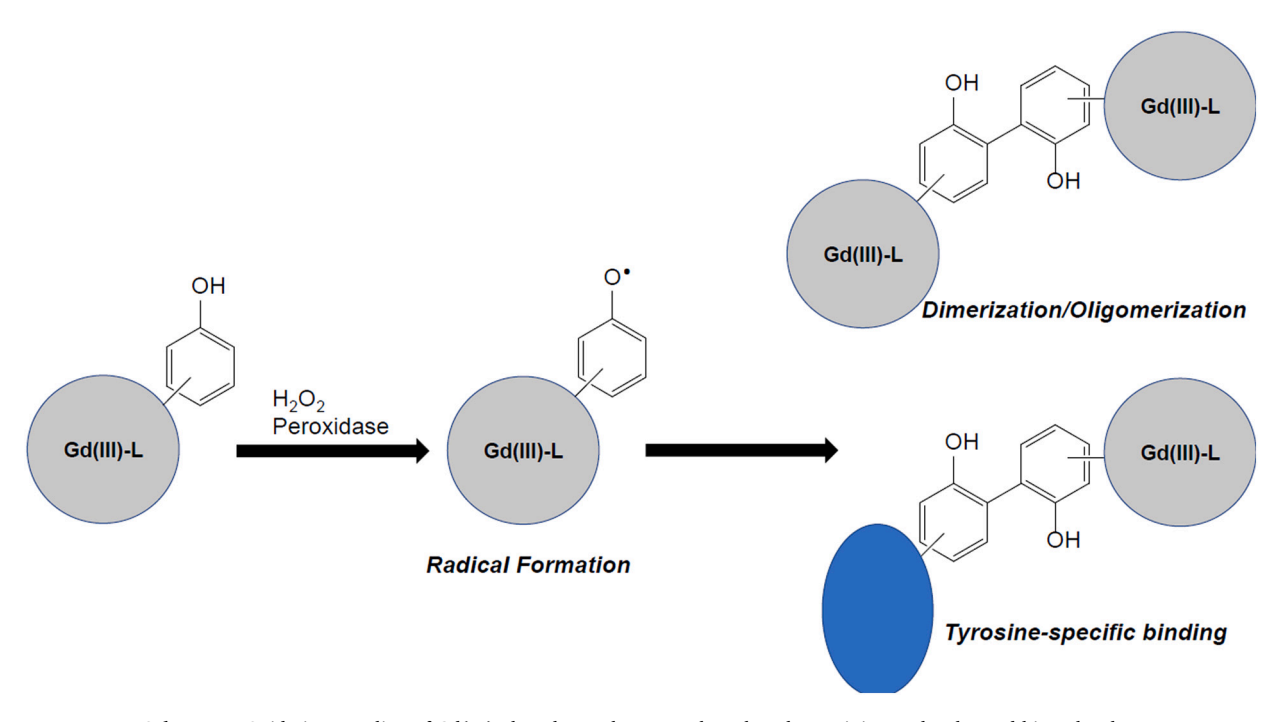
The r_1 of the first studied complex with the D-DOTA³⁻ ligand (Scheme 6) increased 3-fold upon activation by 3.5 mM H₂O₂ and horseradish peroxidase, with a 500 ng/L loading of the enzyme fully oligomerizing the complex within 1 h (0.47 T, 40 °C) [107]. The oligomerization raises r_1 from 3.75 to 11.50 mM⁻¹ s⁻¹. The Gd(III) complexes with the non-macrocyclic ligands DTPA- 1^{3-} and DTPA- 2^{3-} behave similarly and exhibit 3.7- and 2.4-fold enhancements, respectively, under the same conditions [72]. As anticipated, the relaxivity response is field-dependent; the r_1 of the Gd(III) complex with DTPA-1³only increases 1.7-fold when measured in a stronger 1.5 T field. Mass spectrometry analysis of the oligomers isolated from the oxidation reactions suggests that, on average, they consist of either 7 or 8 monomeric units. The Gd(III) complex with the 5-hydroxytryptamidecontaining DTPA-2³⁻ ligand was subsequently used to image MPO activity associated with ischemia-induced inflammation in mice brains [18].

The speed and extent of activation for this class of sensor depend strongly on the choice of the enzyme catalyst. As an alternative to

N N
$$CO_2^-$$
 N $CO_2^ CO_2^ CO_2$

Scheme 5. Structures of the cobalt-binding ligands used in references [98] and [99]. TPA = tris(2-pyridylmethyl)amine.

Scheme 6. Organic ligands for the Gd(III)-containing MRI contrast agent sensors described in references [18,71,72,106,107]. DOTA $^{4-}=2,2',2'',2'''-(1,4,7,10-tetraze)$ tetrazzacyclododecane-1,4,7,10-tetrayl)tetrazacetate; DPTA $^{5-}=$ diethylenetriaminepentaacetate. The displayed ligands have other functional groups in place of one or more of the DOTA $^{4-}=$ and DPTA $^{5-}=$ acetates.



 $\textbf{Scheme 7.} \ \ \text{Oxidative coupling of } \ \ \text{Gd(III)-phenol complexes to other phenol-containing molecules and biomolecules.}$

horseradish peroxidase, Chen et al. investigated the ability of MPO to activate the Gd(III) complexes with D-DOTA³⁻, T-DOTA³⁻, and 5-HT-DOTA³⁻ (Scheme 6) [71]. With this enzyme, the oxidation of the ligands occurs more slowly, and D-DOTA³⁻ did not react to a noticeable extent. The other two ligands were associated with r_I increases ranging from 1.4- to 2-fold with 0.47 and 1.5 T fields, with the larger enhancements again being observed with the weaker 0.47 T field.

Rodríguez et al. later demonstrated that the Gd(III) complexes with the DTPA-1³⁻, DTPA-2³⁻, DTPA-3³⁻, and DTPA-4⁴⁻ ligands (Scheme 6) could potentially covalently tether to tyrosine-containing peptides [106]. MPO was primarily used as the enzyme catalyst; eosinophil peroxidase was also tested but did not promote any oligomerization. Upon reaction with H₂O₂, MPO, and a cysteine-containing polypeptide, the r_1 values of the complexes with DTPA- 2^{3-} , DTPA- 3^{3-} , and DTPA- 4^{4-} increase by 22-59%, with larger gains seen for the latter two ligands. The authors identified a competition between oligomerization and protein cross-linking. The lower response of the DTPA-2³⁻ complex to the peptide was attributed to its preference for oligomerization. In the same publication, Rodríguez et al. demonstrated that these reagents could detect regions with high MPO activity in mouse thighs. In these experiments, the authors embedded MPO within the animals using Matrigel and administered a 0.3 mmol/kg dose of the studied Gd(III) complex. The authors also investigated the cytotoxicity of their probes, finding that NIH-3T3 cells could tolerate concentrations up to 5 mM for the DPTA-3³⁻ and DPTA-4⁴⁻ complexes. In parallel experiments with RAW 264.7 macrophages, which can secrete MPO upon chemical stimulation, the authors found no difference in the viabilities of activated versus non-activated cells, suggesting that the oxidized forms of the sensors were similarly non-toxic.

Tu et al. prepared a Gd(III) complex with a ligand consisting of a spironaphthaoxazine group tethered to 1,4,7,10-tetraazacyclodode-cane-1,4,7-triacetic acid (DO3A) that acts as a turn-on MRI contrast agent sensor for NADH [109]. The coordination of the spironaphthoxazine portion to the Gd(III) is modulated by the redox environment

(Scheme 8). When the Gd(III) complex reacts with NADH, the ligand cyclizes upon reduction, removing the phenol as a potential ligand. This opens a coordination site on the metal center for an additional water molecule. q increases from 1.3 to 2.0 as r_I improves from 5.58 to 8.60 mM $^{-1}$ s $^{-1}$ (60 MHz, 37 °C, pH 7.0 deionized water). The subsequent addition of H_2O_2 in a 3-fold excess relative to the initially added amount of NADH reverses the reaction, both opening the heterocycle and oxidizing the ligand back to the spironaphthaoxazine form. The relaxivity decreases during the H_2O_2 reaction; the compound thereby acts as a turn-off sensor.

Harris et al. synthesized and characterized a Gd(III) complex with a macrocyclic ligand with a redox-active nicotinamide arm (Scheme 9) [110]. The reduced form of the complex has a q of 1.9, leading to a relatively high r_1 of 6.9 mM⁻¹ s⁻¹ (60 MHz, 37 °C, pH 7.0). Upon oxidation of 2 mM of the complex by 20 mM of H₂O₂, q drops to 0.3 and r_1 decreases to 3.7 mM⁻¹ s⁻¹. Harris et al. determined that the presence of bicarbonate was essential for the response; q remains equal within error to the 1.9 value (2.1) when the oxidized sample is instead prepared in solutions that have been rigorously degassed with Ar. The authors speculate that the postive charge of the nicotinimidum in the oxidized form renders the coordination of bicarbonate more favorable by giving the Gd(III) complex an overall charge of +1. The Gd(III) complex with the reduced form of the ligand, conversely, is neutral. The positive charge of the oxidized species is proposed to enable bicarbonate to act as a more competitive inhibitor for water coordination. The oxidation of the ligand can be reversed by dithionite. The results are surprising in that the bicarbonate would be anticipated to bind strongly to the reduced form of the Gd(III) complex despite its lower overall charge.

Work from our own laboratory has focused on preparing manganese-containing MRI contrast agents with redox-active ligands (Scheme 10) [111–117]. Upon reaction with ROS, the metal ion may be oxidized transiently, but the observed changes in the T_I -weighted relaxivity are instead correlated to oxidation-triggered changes in the ligand structure. One benefit to this approach is that one does not need to provide a

Scheme 8. Full structure of the DO3A derivative used as the ligand in the redox-active MRI contrast agent reported in reference [109] and its proposed mode of activation, with a focus on the aquation number of the Gd(III) and the redox-sensitive portion of the ligand. $DO3A^{3-} = 1,4,7,10$ -tetraazacyclododecane-1,4,7-triacetate.

$$H_2O$$
 OH_2 O_2C N N CO_2 O_2C N O_2C N O_2C O_2C

Scheme 9. Proposed mechanism for the r_1 turn-off observed for the Gd(III)-containing probe described in reference [110].

$$H_3C$$
 H_3C
 H_4qp1
 H_4qp2
 H_6qc1
 H_4qp4

Scheme 10. Ligands for the manganese-containing complexes discussed in references [111–117]. Hptp1 = N-(2-hydroxy-5-methyl-benzyl)-N, N', N'-tris(2-pyridinylmethyl)-1,2-ethanediamine; H₂qp1 = N-(2,5-dihydroxybenzyl)-N, N'-bis(2-pyridinylmethyl)-1,2-ethanediamine; H₄qp2 = N, N'-bis(2,5-dihydroxybenzyl)-N, N'-bis(2-pyridinylmethyl)-1,2-ethanediamine; H₆qc1 = N, N'-bis(2,5-dihydroxybenzyl)-ethanediamine-N, N'-diacetic acid; H₄qp4 = 1,8-bis(2,5-dihydroxybenzyl)-1,4,8,11-tetraazacyclotetradecane.

coordination environment that can accommodate two different metal oxidation states. Further, it can enable turn-on r_1 responses with Mn(II) ions.

The Hptp1 ligand features a redox-active para-methylphenol group that will coordinate to Mn(II) as a phenolate at physiological pH [111,112]. In water, the Mn(II) ion ligates a water molecule to form $[Mn^{II}(ptp1)(H_2O)]^+$ [112]. The complex with deprotonated Hptp1 (ptp⁻) rapidly reacts with H₂O₂; during this reaction, the phenolate groups from two separate molecules oxidatively couple together through the carbon atoms ortho to the hydroxides to yield a binuclear Mn(II) species (Scheme 11) [111]. The r_1 per metal center decreases due to the lesser overall paramagnetism of the binuclear cage complex (Table 2). The compound therefore acts as a turn-off sensor for H₂O₂. The ptp complex also behaves as a mimic of superoxide dismutase [112]. During the reactivity with O₂, the same binuclear Mn(II) product is observed as an end-product. The MRI response to O2, however, was not thoroughly analyzed, largely due to the difficulty in deconvoluting the responses of the complex to O_2 and H_2O_2 , the latter of which is a product of the catalyzed superoxide degradation.

Other work from our laboratory has used 1,4-hydroquinones, or quinols, as the redox-active group (Scheme 10) [113–117]. Although this appears at first glance to be a modest change from the para-methylphenol used in Hptp1, the switch from a methyl to a second hydroxy group fundamentally changes the sort of oxidation reaction that preferentially occurs. Instead of coupling two quinols together, the quinols are converted to para-quinones (Scheme 12). Due to their inability to deprotonate to anionic forms, the para-quinones cannot bind to metal centers as avidly and are more readily displaced by water molecules. This increases q and thereby improves r_1 .

The Mn(II) complexes with the H₂qp1, H₄qp2, and H₄qp4 ligands all

react with H_2O_2 to yield Mn(II) species with para-quinone-containing ligands [113,115,117]. The oxidation of the ligand does not go to completion even when a large excess of H_2O_2 is provided, with only 70% of the quinols converting to quinones. The complex with H_4 qp4 has displayed catalase activity [117], and we currently believe that the oxidized complexes can oxidize H_2O_2 and revert to the pre-activated state. With an excess of ROS, the ability to cycle between oxidized and reduced forms leads to an equilibrium mixture of quinol and para-quinone species. As with most of the Mn(II) complexes described in this review, these compounds are mostly air stable, with only $\sim 5\%$ oxidation observed at 18 h, which is much longer than the typical retention time of a MRI contrast agent within the body.

The ligand structure greatly impacts the water stability of the Mn(II) complexes and the magnitude of the relaxivity response. The r_1 of the complex with the monoquinol ligand, $[Mn^{II}(H_2qp1)]^{2+}$, increases by only 10% upon oxidation by H₂O₂ (Table 2) [113]. The H₂qp1 complex is somewhat stable in water, existing mostly as [Mn^{II}(Hqp1)(H₂O)]⁺ above pH 7.00, but its oxidized form readily exchanges its Mn(II) for Zn (II) [113,114]. It is highly likely that physiologically relevant chelators would be able to remove the metal from the sensor in either its preactivated or activated states. The Mn(II) complex with the diquinol ligand H_4 qp2 displays a larger 30% increase in r_1 upon oxidation [115]. The substitution of the second quinol for one of the pyridine rings, however, greatly destabilizes both the reduced and oxidized Mn(II) complexes in water. The oxidation of the H₄qp2 ligand almost certainly leads to dissociation of the Mn(II) from the coordination complex, rendering the sensor impractical for many in vivo applications. Installing carboxylate groups in place of the remaining pyridines yields the H₆qc1 ligand, which coordinates to metal ions as a mixture of the much more anionic H_3qc1^{3-} and H_2qc1^{4-} [116]. Although the [Mn^{II}(H_6qc1)]²⁺ is

much more stable in aqueous solution, the added negative charge renders the metal center more susceptible to oxidation. The reaction with $\rm H_2O_2$ oxidizes both the ligand and metal. The oxidation of the metal to the less paramagnetic Mn(III) counteracts any benefit that the oxidation of the ligand would provide; the $\rm H_6qc1$ complex, consequently, displays essentially no r_1 response to $\rm H_2O_2$.

The inclusion of a macrocycle into the ligand framework markedly improves the stability and unexpectedly enhances the r_1 response to H_2O_2 as well. The speciation of $[Mn^{II}(H_4qp4)]^{2+}$ strongly resembles that of [Mn^{II}(H₄qp2)]²⁺ in that it exists as a mixture of [Mn^{II}(H₃qp4)(H₂O)]⁺ and [Mn^{II}(H₂qp4)(H₂O)] at pH 7.0 [117]. Potentiometric pH titration data for the pre-activated sensor demonstrate that both of these species are extremely stable in water. The kinetic stability of the complex is also excellent. Unlike the H₂qp1 and H₄qp2 complexes with Mn(II), the H₄qp4 species do not readily exchange metal ions with added Fe(II) or Zn(II) in either the pre-activated or oxidized form. The reaction between a large 10 mM excess of H₂O₂ and [Mn^{II}(H₄qp4)]²⁺ differs from those of the H₂qp1 and H₄qp2 systems in that it exhibits an induction period and requires 90 min to reach equilibrium. The induction period has been attributed to competing catalase activity; when a lower amount of H₂O₂ is added, the ligand oxidizes much more quickly. During the reaction, both the measured q and r_1 increase, demonstrating that the ligand oxidation, aquation number, and T1-weighted relaxivity are indeed connected to each other. The relaxivity improves by 130% (Table 2).

The major drawback to these probes is that the pre-activated sensors have high background relaxivities. Although the changes in r_1 for the pre-activated and activated forms are large enough to clearly differentiate the two forms of each of these sensors in *in vitro* samples, it would be difficult to assess *in vivo* whether an enhancement in contrast results from the activation of the probe or the accretion of the reduced form of the compound in a particular region.

3.2. ¹⁹F MRI contrast agent sensors

Recently, there have been many efforts towards preparing sensors with ¹⁹F MRI outputs, some of which are responsive to analytes [73,77,118–121]. The installation of the fluorinated groups needed to provide the MRI signal tends to complicate the syntheses of the organic components. As stated previously, having more F atoms will improve the signal-to-noise ratio, but installing too many F atoms can render the compounds insufficiently soluble in water to use for MRI analysis [76]. As of this writing, all of the redox-responsive sensors with ¹⁹F MRI outputs rely on changes to the oxidation state of the metal ion to provide their spectroscopic response.

With respect to redox-responsive contrast agents that do not react with ROS, Que's group has recently synthesized a series of coppercontaining probes that detect thiols [122–124]. These generally feature less highly paramagnetic metal ions that would be poorly suited for T_1 -weighted 1 H MRI. The key design considerations are the impacts of the metal ions on T_1 and T_2 and the distance between the 19 F atoms and the metal. Optimal paramagnetic enhancement of the 19 F signal seems to occur when the F atoms are 5–7 Å away from the metal center [75].

Chen et al. recently reported a bimodal MRI contrast agent with ¹H and ¹⁹F outputs that consists of manganese bound to *N,N'*-bis(2-

$$-\frac{1}{2}-Mn^{||} -\frac{1}{2}-Mn^{||} + \frac{1}{2}Mn^{||} + \frac{$$

Scheme 11. Depiction of the formation of the binuclear Mn(II) complex from two equiv. of $[Mn^{II}(Hptp1)]^{2+}$. This Scheme also appeared in reference [111].

Table 2 Relaxivities of T_{I} -weighted MRI contrast agents that respond to ROS through changes in the oxidation state of the organic ligand.

| Contrast agent | r_1 (-H ₂ O ₂) (mM ⁻¹ s ⁻¹) | $r_1 (+H_2O_2)$ (mM ⁻¹ s ⁻¹) | r ₁ (+H ₂ O ₂)/r ₁ (-H ₂ O ₂) | Reference |
|---|--|--|--|-----------|
| $\begin{split} &[\text{Mn}^{\text{II}}(\text{Hptp1})]^{2+}\\ &[\text{Mn}^{\text{II}}(\text{H}_2\text{qp1})]^{2+}\\ &[\text{Mn}^{\text{II}}(\text{H}_4\text{qp2})]^{2+}\\ &[\text{Mn}^{\text{II}}(\text{H}_6\text{qc1})]^{2+}\\ &[\text{Mn}^{\text{II}}(\text{H}_4\text{qp4})]^{2+} \end{split}$ | 4.39 | 3.59 ^a | 0.82 | [111] |
| | 4.73 | 5.30 | 1.12 | [113] |
| | 5.46 | 7.17 | 1.31 | [115] |
| | 3.48 ^b | 3.46 ^b | 0.99 | [116] |
| | 3.16 | 7.35 ^c | 2.32 | [117] |

All measurements taken in pH 7.0 HEPES buffer at 25 $^{\circ}$ C with a 3 T field. All of the oxidized samples were treated with 10 mM $\rm H_2O_2$ and measured 30 min after the beginning of the reaction unless otherwise stated.

- ^a This value is per Mn(II) ion.
- ^b Measurements taken in pH 7.0 50 mM phosphate buffer.
- ^c Measurement taken 90 min after the reaction with 10 mM H₂O₂.

hydroxy-4-trifluoromethylbenzyl)-ethylenediamine-N,N'-diaceticacid (HTFBED, Scheme 13) [95]. The coordination of Mn(III) to the ligand results in an 8-fold intensification of its $^{19}{\rm F}$ NMR signal. Coordinating Mn(II) to the ligand, conversely, essentially eliminates the $^{19}{\rm F}$ signal. As with the manganese-containing redox-responsive MRI contrast agents reported by the Gale and Caravan groups [84–86], the r_I associated with the $^{1}{\rm H}$ MRI signal decreases to 26% of its original value upon oxidation of the metal center from Mn(II) to Mn(III) (Table 1). A $^{19}{\rm F}$ MRI signal, conversely, appears as the Mn(II) compound is oxidized by ${\rm H_2O_2}$. Chen et al. used their Mn(II) complex to successfully detect pyocyanin-induced ROS production in HepG2 cells.

Yu et al. reported a series of Co(II) complexes with fluorinated derivatives of 1,4,7-triazacyclononane (TACN) that produce a strong 19 F MRI signal upon oxidation by $\rm H_2O_2$ [125,126]. The pre-activated Co(II) species are high-spin; much like high-spin Mn(II), these metal ions can shorten the T_2 relaxation time and attenuate the 19 F MRI signal. The reaction with $\rm H_2O_2$ oxidizes the metal center to diamagnetic low-spin Co (III); this eliminates the paramagnetic relaxation enhancement, lengthens T_2 , and produces a strong 19 F MRI signal.

The TACN framework endows the Co(II) and Co(III) compounds with great measures of thermodynamic and kinetic stability [125,126]. The Co(II) complex with 1,4,7-triazacyclononanetriacetic acid is airsensitive [127], necessitating that the authors carefully modify the TACN ring in order to avoid O_2 reactivity (Scheme 13) [125,126]. The initially explored complex, [Co^{II}(NODA-CF₃)], reacts relatively slowly with H_2O_2 , and 30 min are required for 4 equiv. of the oxidant to fully activate the sensor [125]. Upon oxidation to Co(III), the ¹⁹F MRI signal intensifies over 2-fold. The T_1 and T_2 values for the Co(II) form are 18.0 and 6.6 ms, respectively; these values are different enough to flatten the ¹⁹F NMR peak and weaken the MRI signal. Yu et al. surveyed a number of oxidants and found that O_2 and ONOO , but not ClO and *tert*-butyl hydroperoxide, could also trigger the response. The reactions involving the former two oxidants, however, proceeded more slowly than those with H_2O_2 .

The L1 and L2 ligands (Scheme 13) contain more F atoms and should thereby give rise to stronger 19 F MRI signals [126]. Despite the two ligands sharing some structural features with NODA-CF3, the Co(II) complexes with L1 and L2 behave quite differently with respect to their 19 F NMR and MRI behavior in that their T_I and T_2 values are

$$HO$$
 H_2O_2
 H_2O_3
 H_2O_4
 H_2O_5
 H_2O_6
 H_2O_6
 H_2O_6

Scheme 12. Illustration of the oxidation of the Mn(II)-quinolate to a Mn(II)-aqua species with a detached *para*-quinone.

$$F_{3}C$$

$$O_{2}C$$

$$O_{2}C$$

$$O_{3}C$$

$$O_{2}C$$

$$O_{3}C$$

$$O_{2}C$$

$$O_{3}C$$

$$O_{4}C$$

$$O_{5}C$$

$$O_{5}C$$

$$O_{7}C$$

$$O_{7}C$$

$$O_{7}C$$

$$O_{8}C$$

$$O$$

Scheme 13. Fluorinated ligands used for the 19 F MRI contrast agent sensors for ROS described in references [95,125,126]. HTFBED $^{4-}$ = N,N'-bis(4-tri-fluoromethylphenolate)ethylenediamine-N,N'-diacetate; NODA-CF $_3$ = 4,7-bis(acetate)-1,4,7-triazacyclononane-1-N-(2,2,2-trifluoroethylacetamide; L1 = 2,2'-(7-(2-((2-((1,1,1,3,3,3-hexafluoro-2-(trifluoromethyl)propan-2-yl)oxy)ethyl)amino)-2-oxoethyl)-1,4,7-triazonane-1,4-diyl)diacetate; L2 = 2-(4,7-bis((1H-pyrazol-3-yl)methyl)-1,4,7-triazonan-1-yl)-N-(2-((1,1,1,3,3,3-hexafluoro-2-(trifluoromethyl)propan-2-yl)oxy)ethyl)acetamide.

approximately equal to each other. Consequently, strong $^{19}\mathrm{F}$ MRI signals are seen for the pre-activated sensors. When the L1 and L2 complexes are oxidized by excess H_2O_2 , the frequencies of the $^{19}\mathrm{F}$ NMR peaks shift by almost 10 ppm. The large magnitude of the shift was attributed to the trigonal prismatic geometries of the compounds which provide greater magnetic anisotropies than the more commonly seen octahedral coordination environments; this phenomenon has been documented for other Co(II) complexes [128–130]. Yu et al. confirmed the hypothesized anisotropy of their complexes using variable temperature magnetic susceptibility measurements [126]. The sensor can thereby ratiometrically detect ROS by using different excitation pulses to separately visualize the Co(II) and Co(III) forms of the sensor. The authors also found that the complex with L2, but not L1, could successfully detect the low steady-state levels of H_2O_2 generated from the reaction between glucose oxidase and glucose.

3.3. CEST-based MRI contrast agent sensors

Several redox-active MRI contrast agents have been developed that rely on CEST for their response. Sherry's group, for instance, reported two Eu(III)-containing complexes that react with reductants [131,132]. The coordination compounds described in this section can respond to oxidants through changes to the oxidation states of either their metal ions or their organic ligands.

3.3.1. Sensors that rely on a change to the oxidation state of the metal ion

The Co(III/II) redox couple would be ideal for a ROS sensor that relies on PARACEST. Co(II) in either its high-spin or low-spin forms is paramagnetic, whereas octahedral Co(III) complexes have a strong tendency to be low-spin and diamagnetic [108]. Oxidizing a CEST-active probe containing Co(II) to a Co(III) species would be anticipated to eliminate the paramagnetically shifted resonance peaks required for PARACEST and result in an enhancement of the water signal – a turn-on response [54]. The Co(III/II) reduction potential can be tuned to enable Co(II) compounds to be oxidized by a variety of oxidants. Although this has not yet been applied towards the development of a sensor that is selective for H₂O₂ over O₂, it should be feasible.

Scheme 14. Structure of the ligand used in the CEST-based cobalt-containing sensor described in reference [133]. TPT=1,4,7-tris(pyrazol-3-ylmethyl)-1,4,7-triazacyclononane.

TPT

The Morrow group prepared a Co(II)-containing sensor that loses its ability to participate in PARACEST upon its oxidation to a Co(III) complex by O₂ [133]. Tsitovich et al. synthesized a high-spin Co(II) complex with the TPT ligand (Scheme 14). Proton exchange between the pyrazole groups on the ligand and the bulk water is proposed to enable CEST. The chemical shift of the pyrazole protons is temperaturedependent, decreasing from 149 ppm at 25 °C to a value of 140 ppm at 37 °C. At 37 °C, the optimal frequency offset is 135 ppm. The frequency offset is not impacted by pH, but the magnitude of the CEST effect is, being most prominent at pH 6.9. Upon oxidation by air, the NMR features associated with the Co(II) complex vanish, and CEST no longer occurs with the 135 ppm presaturation pulse. The reaction with O₂ occurs moderately quickly, with a second-order rate constant of 0.32 M^{-1} s⁻¹. The authors estimate that the Co(II)-TPT complex would have a half-life of 2.6 h in arterial blood, approximating the concentration of O₂ as 0.17 mM under these conditions. The Co(III) form of the sensor can be reduced back to Co(II) with dithionite, but the oxidation of Co(II) by H₂O₂ was not investigated.

The Allen group has explored a series of redox-responsive MRI contrast agents that rely on Eu(III/II) redox couples [101-105]. Eu(II) is isoelectronic to Gd(III) and likewise can endow coordination complexes with high r_1 values that are suitable for T_1 -weighted MRI. Although it is still relatively paramagnetic, Eu(III) has a slow water exchange rate and does not significantly impact T_1 ; instead, this ion greatly shifts the NMR signals of nearby protons, including those from bound ligands that can exchange with those from the bulk water. Eu(III) is therefore highly suitable for PARACEST. The use of a fluorinated ligand (Scheme 15) can also enable redox-responsive ¹⁹F MRI. Eu(III) complexes with such ligands can give rise to strong ¹⁹F MRI signals whereas Eu(II) species are 19 F MRI silent [105]. The ability to facilely support multimodal imaging makes the Eu(III/II) couple highly attractive for redox-responsive probes. The key challenge with these sensors is that the Eu(II) oxidation state tends to be highly unstable. Even when they can be sufficiently stabilized under anaerobic environments, most Eu(II) complexes react quickly with air [101–105] and only persist under hypoxic conditions, such as the necrotic interiors of tumors [103].

Funk et al. prepared a Eu(II) complex with DOTA(gly)₄⁴⁻ that oxidizes to a Eu(III) species upon reaction with H₂O₂ over the course of 1 h (Scheme 16) [134]. Most Eu(II) complexes are highly reactive [108], and the amide groups of the DOTA(gly)₄⁴⁻ ligand were installed to improve the redox stability of the Eu(II) form. Indeed, the Eu(III/II) reduction potential was measured to be -226 mV vs. Ag+/AgCl as opposed to -585 mV for the Eu(II) agua ion. The amide groups also provide protons that can exchange with the bulk water; the frequency offset for the ligand protons is +54 ppm. The Eu(II) complex has a r_1 of 3.2 mM $^{-1}$ s $^{-1}$ (1 T, pH 7.0). During its oxidation by H₂O₂, the T_1 weighted signal from the Eu(II) fades while the CEST-based effect from the Eu(III) manifests. The maximum CEST effect for a 10 mM sample of the Eu(III) complex results in a 27% decrease of the water signal. The Eu (II) complex displays a similar, but slower, response to O2. Eliminating the side reactivity with O2 remains a significant barrier in using Eu(III/ II) couples as the basis for H₂O₂-selective sensors.

Scheme 15. Ligands used in the preparation of the air-responsive Eu(II) complexes described in references [101–105].

Scheme 16. The europium-containing sensor that responds to oxidation with changes to both its T₁-weighted and CEST signals described in reference [134].

Scheme 17. Ligands for the diiron complex described in reference [135].

Du et al. reported a binuclear Fe(II) complex with a tetra(carboxamide) ligand (Scheme 17) and etidronate [135]. The metal ions in [Fe₂(L)(etidronate)] can be oxidized, yielding either Fe(II)Fe(III) or Fe (III)₂ species. The carboxamide groups on the polydentate ligand can exchange protons with water, allowing the Fe(II)2 and Fe(II)Fe(III) complexes to engage in CEST. At 37 °C and pH 7.4, the diferrous complex has CEST peaks at +29, +40, and +68 ppm; excitation at these frequencies reduces the water signal by approximately 9%, 10%, and 5%, respectively. The Fe(II)Fe(III) complex is more effective as a PAR-ACEST reagent, and the water signal decreases in intensity by approximately 20% when peaks at either +74 or +83 ppm are irradiated. Selective irradiation can therefore distinguish the Fe(II)2 and Fe(II)Fe (III) species. As with other PARACEST agents, the intensities and the frequency offsets of the CEST peaks are influenced by pH and temperature. With respect to the impact of temperature, a 2 °C change was found to shift the 83 ppm CEST peak of the Fe(II)Fe(III) complex by 1 ppm.

Oxidation of 4 mM of $[Fe^{II}_2(L)(etidronate)]^-$ by a substoichiometric amount (1 mM) of KO_2 in pH 7.4 buffer partly oxidizes the complex to the Fe(II)Fe(III) species. The reaction occurs quickly, reaching equilibrium in under 10 min. With proper ligand modifications, such a diiron system could be tuned towards the selective detection of H_2O_2 .

3.3.2. Sensors that rely on a change to the oxidation state of the organic ligand

Thus far, there are no known examples of CEST-based sensors that detect $\rm H_2O_2$ through changes to their organic portions. Nonetheless, this is one avenue that could be explored further as the following two cases demonstrate.

Liu et al. prepared a Yb(III) complex with the redox-active macrocyclic ligand DO3A-oAA (Scheme 18) [136]. The compound exhibits two CEST peaks at -11 ppm and + 8 ppm that are attributed to the amide and amine groups, respectively. The CEST effect from the amine protons can decrease the water signal by as much as 30%, with the maximum impact observed at pH 5. The amide protons can decrease the water intensity by as much as 20%, with the optimal effect observed at pH 7. Upon reaction with a mixture of NO and O₂, the aniline groups of two equiv. of the Yb(III) complex irreversibly combine into a triazene bridge (Scheme 18). After the ligand oxidation, neither the -11 ppm nor the +8 ppm CEST effects are observed. The loss of the amine protons accounts for the elimination of the +8 ppm signal, but the disappearance of the amide-based signal was unanticipated. The authors speculate that the ligand oxidation triggers a conformational change that moves the amides far enough away from the Yb(III) ions to eliminate the paramagnetic shift needed for efficient PARACEST.

Song et al. synthesized a Eu(III)-containing sensor with a redoxactive anthracene that exhibits a response that is selective for singlet oxygen (Scheme 19) [137]. In the reduced form, the Eu(III) complex exhibits a CEST signal at +50 ppm that attenuates the water intensity by approximately 8%. Reaction with chemically generated $^{1}O_{2}$ converts the anthracene into a peroxide and shifts the frequency of the nearby amide proton to +53 ppm. The CEST effect for the oxidized complex is stronger, with approximately a 12% decrease in the intensity of the water signal. Song et al. investigated other ROS but did not observe any change to the CEST properties with either ONOO $^{-}$, $H_{2}O_{2}$, OH, or O_{2}^{-} . The authors were able to use the ratio of the CEST effects at +54 and +47 ppm to monitor the production of singlet oxygen in phantom samples and cell lysates from HeLa cells.

 $\textbf{Scheme 18.} \ \ \textbf{Yb(III)-containing sensor for NO/O}_2 \ \ \textbf{mixtures from reference [136].} \ \ \textbf{DO3A-oAA} \ = \ 1,4,7,10\text{-tetraazacyclododecane-1},4,7\text{-triacetic acid} - \text{orthoaminoanilide.}$

Scheme 19. Eu(III)-containing sensor for singlet oxygen described in reference [137].

4. Conclusions and outlook

Small molecule MRI contrast agent sensors for ROS, such as $\rm H_2O_2$, continue to be developed at a rapid pace. Recent progress in this field has benefitted from the exploration of new modes of MRI, specifically $^{19}\rm F$ and CEST. The sensors described here are incredibly diverse with respect to the metal ions and ligand structures employed. Some of the organic components include redox-active functional groups that can be oxidized to either couple the sensor to another molecule, effect changes in the coordination sphere of the metal ion, or alter the resonance frequencies of protons participating in CEST.

This said, there remain several challenges that need to be overcome before any of these probes can enter clinical use and possibly diagnose health conditions from patterns of abnormal oxidative activity. Some of these challenges are general and apply to all potential sensors. How toxic are the probes in both their pre-activated and activated states? Where do they accumulate in the body and how quickly do they clear these areas? Can they encounter enough $\rm H_2O_2$, react with it quickly enough, and provide a sufficiently large change in the signal to clearly differentiate a region experiencing oxidative stress? The timescale of the reaction is particular important if the probes are freely circulating through the body.

These general challenges may be more acute for certain classes of probes. Coordination complexes with redox-active metal ions that can participate in Fenton-like chemistry, such as manganese and iron, would be anticipated to be more toxic than those with redox-inactive metals. Complexes with weak stability constants would have a stronger tendency to release free metal ions, which would also worsen the toxicity. The probes that are capable of tethering to biomolecules could potentially target tissues of interest but may clear the body less avidly. Those that oligomerize risk becoming insoluble. Most of the complexes described here are not likely to be lipophilic enough to enter cells; indeed, this is perhaps for the better since high lipophilicity would be expected to impede the clearance of the contrast agent from the body. MRI contrast agent sensors will instead likely react with the H₂O₂ that diffuses into extracellular spaces. Fortunately, the successful use of some of these sensors in biological imaging suggests that enough ROS do make

it to these spaces to enable MRI to detect aberrant oxidative activity.

Other challenges are specific to individual spectroscopic techniques. With T_1 -weighted MRI, it is difficult to differentiate sensor activation from accumulation of the lower-relaxivity form of the probe. These probes can be used to detect oxidative stress, but only after their performance has been carefully and systematically calibrated in populations of physiologically healthy and unhealthy tissues. The same issue applies to arguably a lesser extent with ¹⁹F MRI-based sensors, but with these, a much higher loading of the contrast agent is generally needed, exacerbating concerns about toxicity. Given the solubility difficulties that arise upon further fluorinating small molecules, the need for a high dose of a ¹⁹F MRI contrast agent may be a rarely surmounted obstacle. With CEST, the more intense irradiation needed to acquire an unambiguous signal represents a substantial technical challenge, but it may be overcome through making changes to how the irradiation is provided. With respect to using CEST as the basis for redox-responsive MRI, the temperature- and pH-dependencies of the CEST effect will further complicate calibration and the determination of what an observed change in the signal may actually mean.

The necessary calibration may be much simpler for multimodal sensors. With multiple spectroscopic signatures that can separately visualize the pre-activated and activated states, one can readily assess sensor distribution and the extent to which the probes have been activated. Ultimately, such probes may have a slightly easier path to being applied fruitfully in the clinic.

Author statement

Sana Karbalaei: Formulated the idea for the review, wrote the original draft, edited and revised subsequent drafts.

Christian R. Goldsmith: Formulated the idea for the review, wrote the original draft, edited and revised subsequent drafts, and acquired funding to support authors during the composition of the manuscript.

Declaration of Competing Interest

The authors declare that they have no known competing financial

interests or personal relationships that could have appeared to influence the work reported in this paper.

Acknowledgements

S. K. was supported by Auburn University and the National Science Foundation (NSF-CHE-1954336) during the composition of this review. We thank Dr. Ronald J. Beyers for his assistance with the revision of the manuscript. C. R. G. is deeply indebted to the late Prof. Richard H. Holm for his undergraduate mentorship.

References

- N.A. Stefanova, N.A. Muraleva, V.P. Skulachev, N.G. Kolosova, J. Alzheimers Dis. 38 (2014) 681–694.
- [2] V.P. Skulachev, J. Alzheimers Dis. 28 (2012) 283-289.
- [3] V.I. Lushchak, Chem. Biol. Interact. 224 (2014) 164-175.
- [4] I.A. Abreu, D.E. Cabelli, Biochim. Biophys. Acta 1804 (2010) 263–274.
- [5] K. Wieghardt, Angew. Chem. Int. Ed. 28 (1989) 1153-1172.
- [6] S. Mukhopadhyay, S.K. Mandal, S. Bhaduri, W.H. Armstrong, Chem. Rev. 104 (2004) 3981–4026.
- [7] R.H. Holm, P. Kennepohl, E.I. Solomon, Chem. Rev. 96 (1996) 2239–2314.
- [8] G.S.A.T. van Rossum, G.P.C. Drummen, A.J. Verkleij, J.A. Post, J. Boonstra, Biochim. Biophys. Acta 1636 (2004) 183–195.
- [9] A. Vaarmann, S. Gandhi, A.Y. Abramov, J. Biol. Chem. 285 (2010) 25018–25023.
- [10] M. Sundaresan, Z.-X. Yu, V.J. Ferrans, K. Irani, T. Finkel, Science 270 (1995) 296–299.
- [11] H.A. Woo, S.H. Yim, D.H. Shin, D. Kang, D.-Y. Yu, S.G. Rhee, Cell 140 (2010) 517–528.
- [12] P.R. Angelova, W.S. Müller, Eur. J. Neurosci. 29 (2009) 1943-1950.
- [13] P. Angelova, W. Müller, Eur. J. Neurosci. 23 (2006) 2375–2384.
- [14] L.C. Hool, B. Corry, Antioxid. Redox Signal. 9 (2007) 409-435.
- [15] H.J. Forman, J.M. Fukuto, M. Torres, Am. J. Phys. Cell Phys. 287 (2004) C246–C256.
- [16] H.J. Forman, M. Maiorino, F. Ursini, Biochemistry 49 (2010) 835-842.
- [17] A.N. Lyle, K.K. Griendling, Physiology 21 (2006) 269-280.
- [18] M.O. Breckwoldt, J.W. Chen, L. Stangenberg, E. Aikawa, E. Rodriguez, S. Qiu, M. A. Moskowitz, R. Weissleder, Proc. Nat. Acad. Sci., U. S. A. 105 (2008) 18584–18589
- [19] V.L. Kinnula, Curr. Drug Targets. Inflamm. Allergy 4 (2005) 465–470.
- [20] M.I. Ahmed, J.D. Gladden, S.H. Litovsky, S.G. Lloyd, H. Gupta, S. Inusah, T. Denney Jr., P. Powell, D.C. McGiffin, L.J. Dell'Italia, J. Am. Coll. Cardiol. 55 (2010) 671–679.
- [21] J.D. Gladden, M.I. Ahmed, S.H. Litovsky, C.G. Schiros, S.G. Lloyd, H. Gupta, T. S. Denney Jr., V. Darley-Usmar, D.C. McGiffin, L.J. Dell'Italia, Am. J. Med. Sci. 342 (2011) 114–119.
- [22] K. Gaddam, C. Corros, E. Pimenta, M. Ahmed, T. Denney, I. Aban, S. Inusah, H. Gupta, S.G. Lloyd, S. Oparil, A. Husain, L.J. Dell'Italia, D.A. Calhoun, Hypertension 55 (2010) 1137–1142.
- [23] S. Viappiani, R. Schulz, Am. J. Physiol. Heart Circ. Physiol. 290 (2006) H2167–H2168.
- [24] I.M. Fearon, S.P. Faux, J. Mol. Cell. Cardiol. 47 (2009) 372-381.
- [25] J. van Horssen, M.E. Witte, G. Schreibelt, H.E. de Vries, Biochim. Biophys. Acta 1812 (2011) 141–150.
- [26] J.-Y. Wang, L.-L. Wen, Y.-N. Huang, Y.-T. Chen, M.-C. Ku, Curr. Pharm. Des. 12 (2006) 3521–3533.
- [27] L. Tretter, I. Sipos, V. Adam-Vizi, Neurochem. Res. 29 (2004) 569-577.
- [28] R.L. Mosley, E.J. Benner, I. Kadiu, M. Thomas, M.D. Boska, K. Hasan, C. Laurie, H. E. Gendelman, Clin. Neurosci. Res. 6 (2006) 261–281.
- [29] M.Y. Askenov, M.V. Askenova, D.A. Butterfield, J.W. Geddes, W.R. Markesbery, Neurosci. 103 (2001) 373–383.
- [30] D.P. Riley, W.J. Rivers, R.H. Weiss, Anal. Biochem. 196 (1991) 344-349.
- [31] I. Fridovich, J. Biol. Chem. 272 (1997) 18515–18517.
- [32] M. Giorgio, M. Trinei, E. Migliaccio, P.G. Pelicci, Nat. Rev. Mol. Cell Biol. 8 (2007) 722–728.
- [33] F. Haber, J. Weiss, Naturwissenschaften 20 (1932) 948-950.
- [34] H.J.H. Fenton, J. Chem. Soc. Trans. 65 (1894) 899-910.
- [35] S. Aime, M. Botta, E. Gianolio, E. Terreno, Angew. Chem. Int. Ed. 39 (2000) 747–750.
- [36] S. Aime, M. Botta, S.G. Crich, G.B. Giovenzana, R. Pagliarin, M. Piccinini, M. Sisti, E. Terreno, J. Biol. Inorg. Chem. 2 (1997) 470–479.
- [37] J.L. Major, T.J. Meade, Acc. Chem. Res. 42 (2009) 893–903.
- [38] J. Lee, M.J. Zylka, D.J. Anderson, J.E. Burdette, T.K. Woodruff, T.J. Meade, J. Am. Chem. Soc. 127 (2005) 13164–13166.
- [39] J.L. Major, G. Parigi, C. Luchinat, T.J. Meade, Proc. Natl. Acad. Sci. U. S. A. 104 (2007) 13881–13886.
- [40] X.-a. Zhang, K.S. Lovejoy, A. Jasanoff, S.J. Lippard, Proc. Natl. Acad. Sci. U. S. A. 104 (2007) 10780–10785.
- [41] E. Kawabata, K. Kikuchi, Y. Urano, H. Kojima, A. Odani, T. Nagano, J. Am. Chem. Soc. 127 (2005) 818–819.
- [42] T. Hirano, K. Kikuchi, Y. Urano, T. Higuchi, T. Nagano, J. Am. Chem. Soc. 122 (2000) 12399–12400.

- [43] S. Maruyama, K. Kikuchi, T. Hirano, Y. Urano, T. Nagano, J. Am. Chem. Soc. 124 (2002) 10650–10651.
- [44] K.P. Divya, S. Sreejith, P. Ashokkumar, K. Yuzhan, Q. Peng, S.K. Maji, Y. Tong, H. Yu, Y. Zhao, P. Ramamurthy, A. Ajayaghosh, Chem. Sci. 5 (2014) 3469–3474.
- [45] A. Torrado, G.K. Walkup, B. Imperiali, J. Am. Chem. Soc. 120 (1998) 609-610.
- [46] J. Zhang, R.E. Campbell, A.Y. Ting, R.Y. Tsien, Nat. Rev. Mol. Cell Biol. 3 (2002) 906–918.
- [47] B.A. Griffen, S.R. Adams, R.Y. Tsien, Science 281 (1998) 269-272.
- [48] L.M. De Leon-Rodriguez, A.J.M. Lubag, C.R. Malloy, G.V. Martinez, R.J. Gillies, A. D. Sherry, Acc. Chem. Res. 42 (2009) 948–957.
- [49] J. Wahsner, E.M. Gale, A. Rodríguez-Rodríguez, P. Caravan, Chem. Rev. 119 (2019) 957–1057.
- [50] S.M. Pinto, V. Tomé, M.J.F. Calvete, M.M.C.A. Castro, É. Tóth, C.F.G.C. Geraldes, Coord. Chem. Rev. 390 (2019) 1–31.
- [51] Q.N. Do, J.S. Ratnakar, Z. Kovács, A.D. Sherry, ChemMedChem 9 (2014) 1116–1129.
- [52] S. Zhang, M. Merritt, D.E. Woessner, D.E. Lenkinski, A.D. Sherry, Acc. Chem. Res. 36 (2003) 783–790.
- [53] P.B. Tsitovich, P.J. Burns, A.M. McKay, J.R. Morrow, J. Inorg. Biochem. 133 (2014) 143–154.
- [54] A.K. Renfrew, E.S. O'Neill, T.W. Hambley, E.J. New, Coord. Chem. Rev. 375 (2018) 221–233.
- [55] P. Caravan, J.J. Ellison, T.J. McMurry, R.B. Lauffer, Chem. Rev. 99 (1999) 2293–2352.
- [56] E. Tóth, L. Helm, A.E. Merbach, Top. Curr. Chem. 221 (2002) 61-101.
- [57] B. Drahoš, I. Lukeš, É. Tóth, Eur. J. Inorg. Chem. 2012 (2012) 1975–1986.
- [58] E.M. Gale, I.P. Atanasova, F. Blasi, I. Ay, P. Caravan, J. Am. Chem. Soc. 137 (2015) 15548–15557.
- [59] J.S. Troughton, M.T. Greenfield, J.M. Greenwood, S. Dumas, A.J. Wiethoff, J. Wang, M. Spiller, T.J. McCurry, P. Caravan, Inorg. Chem. 43 (2004) 6313–6323.
- [61] S.M. Rocklage, W.P. Cacheris, S.C. Quay, F.E. Hahn, K.N. Raymond, Inorg. Chem. 28 (1989) 477–485.
- [62] S. Aime, S. Baroni, D. Delli Castelli, E. Brücher, I. Fábián, S.C. Serra, A. Fringuello Mingo, R. Napolitano, L. Lattuada, F. Tedoldi, Z. Baranyai, Inorg. Chem. 57 (2018) 5567–5574.
- [63] J.A. Duimstra, F.J. Femia, T.J. Meade, J. Am. Chem. Soc. 127 (2005) 12847–12855.
- [64] D.D. Schwert, J.A. Davies, N. Richardson, Top. Curr. Chem. 221 (2002) 165–199.
- [65] E.M. Snyder, D. Asik, S.M. Abozeid, A. Burgio, G. Bateman, S.G. Turowski, J. A. Spernyak, J.R. Morrow, Angew. Chem. Int. Ed. 59 (2020) 2414–2419.
- [66] B.-A. Hoener, B.L. Engelstad, E.C. Ramos, H.A. Macapinlac, D.C. Price, T. R. Johnson, D.L. White, J. Magn. Reson. 1 (1991) 357–362.
- [67] M. Regueiro-Figueroa, G.A. Rolla, D. Esteban-Gómez, A. de Blas, T. Rodríguez-Blas, M. Botta, C. Platas-Iglesias, Chem. Eur. J. 20 (2014) 17300–17305.
- [68] V. Jacques, S. Dumas, W.-C. Sun, J.S. Troughton, M.T. Greenfield, P. Caravan, Investig, Radiol. 45 (2010) 613–624.
- [69] Q. Zhang, J.D. Gorden, R.J. Beyers, C.R. Goldsmith, Inorg. Chem. 50 (2011) 9365–9373.
- [70] A. Gupta, P. Caravan, W.S. Price, C. Platas-Iglesias, E.M. Gale, Inorg. Chem. 59 (2020) 6648–6678.
- [71] J.W. Chen, W. Pham, R. Weissleder, A. Bogdanov Jr., Magn. Reson. Med. 52 (2004) 1021–1028.
- [72] M. Querol, J.W. Chen, R. Weissleder, A. Bogdanov, Org. Lett. 7 (2005) 1719–1722.
- [73] D. Xie, M. Yu, R.T. Kadakia, E.L. Que, Acc. Chem. Res. 53 (2020) 2–10.
- [74] I. Tirotta, V. Dichiarante, C. Pigliacelli, G. Cavallo, G. Terraneo, F.B. Bombelli, P. Metrangolo, G. Resnati, Chem. Rev. 115 (2015) 1106–1129.
- [75] K.L. Peterson, K. Srivastava, V.C. Pierre, Front. Chem. 6 (2018) 160.
- [76] R. Díaz-López, N. Tsapis, E. Fattal, Pharm. Res. 27 (2009) 1.
- [77] A. Sarkar, I.E. Biton, M. Neeman, A. Datta, Inorg. Chem. Commun. 78 (2017) 21–24.
- [78] P.C.M. van Zijl, N.N. Yadav, Magn. Reson. Med. 65 (2011) 927–948.
- [79] K.M. Ward, A.H. Aletras, R.S. Balaban, J. Magn. Reson. 143 (2000) 79–87.
- [80] B. Wu, G. Warnock, M. Zaiss, C. Lin, M. Chen, Z. Zhou, L. Mu, D. Nanz, R. Tuura, G. Delso, EJNMMI Phys. 3 (2016) 19.
- [81] L.H. Bryant, M.W. Hodges, R.G. Bryant, Inorg. Chem. 38 (1999) 1002-1005.
- [82] G. Hernandez, R.G. Bryant, Bioconjug. Chem. 2 (1991) 394–397.
- [83] S.M.A. Pinto, M.J.F. Calvete, M.E. Ghica, S. Soler, I. Gallardo, A. Pallier, M. B. Laranjo, A.M.S. Cardoso, M.M.C.A. Castro, C.M.A. Brett, M.M. Pereira, É. Tóth, C.F.G.C. Geraldes, Dalton Trans. 48 (2019) 3249–3262.
- [84] G.S. Loving, S. Mukherjee, P. Caravan, J. Am. Chem. Soc. 135 (2013) 4620-4623.
- [85] E.M. Gale, S. Mukherjee, C. Liu, G.S. Loving, P. Caravan, Inorg. Chem. 53 (2014) 10748–10761.
- [86] E.M. Gale, C.M. Jones, I. Ramsay, C.T. Farrar, P. Caravan, J. Am. Chem. Soc. 138 (2016) 15861–15864.
- [87] H. Wang, V.C. Jordan, I.A. Ramsay, M. Sojoodi, B.C. Fuchs, K.K. Tanabe, P. Caravan, E.M. Gale, J. Am. Chem. Soc. 141 (2019) 5916–5925.
- [88] E.M. Gale, J. Zhu, P. Caravan, J. Am. Chem. Soc. 135 (2013) 18600–18608.[89] J. Oakes, E.G. Smith, J. Chem. Soc. Faraday Trans. 2 77 (1981) 299–308.
- [90] S. Richards, B. Pedersen, J.V. Silverton, J.L. Hoard, Inorg. Chem. 3 (1964) 27-33.
- [91] M.S. Zetter, M.W. Grant, E.J. Wood, H.W. Dodgen, J.P. Hunt, Inorg. Chem. 11 (1972) 2701–2706.
- [92] A.E. Frost, H.H. Freedman, S.J. Westerback, A.E. Martell, J. Am. Chem. Soc. 80 (1958) 530–536.
- [93] R. Banerjee, J. Biol. Chem. 287 (2012) 4397-4402.

- [94] A.E. Martell, Critical Stability Constants, Plenum Press, New York, NY, 1974.
- [95] H. Chen, X. Tang, X. Gong, D. Chen, A. Li, C. Sun, H. Lin, J. Gao, Chem. Commun. 56 (2020) 4106–4109.
- [96] J.C. Gore, Y.S. Kang, Phys. Med. Biol. 29 (1984) 1189-1197.
- [97] S.-P. Ding, J.-C. Li, C. Jin, World J. Gastroenterol. 9 (2003) 584-589.
- [98] E.S. O'Neill, J.L. Kolanowski, G.H. Yin, K.M. Broadhouse, S.M. Grieve, A. K. Renfrew, P.D. Bonnitcha, E.J. New, RSC Adv. 6 (2016) 30021–30027.
- [99] E.S. O'Neill, A. Kaur, D.P. Bishop, D. Shishmarev, P.W. Kuchel, S.M. Grieve, G. A. Figtree, A.K. Renfrew, P.D. Bonnitcha, E.J. New, Inorg. Chem. 56 (2017) 9860–9868.
- [100] P. Caravan, É. Tóth, A. Rockenbauer, A.E. Merbach, J. Am. Chem. Soc. 121 (1999) 10403–10409.
- [101] L.A. Ekanger, D.R. Mills, M.M. Ali, L.A. Polin, Y. Shen, E.M. Haacke, M.J. Allen, Inorg. Chem. 55 (2016) 9981–9988.
- [102] L.A. Ekanger, M.M. Ali, M.J. Allen, Chem. Commun. 50 (2014) 14835–14838.
- [103] L.A. Ekanger, L.A. Polin, Y. Shen, E.M. Haacke, P.D. Martin, M.J. Allen, Angew. Chem. Int. Ed. 54 (2015) 14398–14401.
- [104] L.A. Basal, Y. Yan, Y. Shen, E.M. Haacke, M. Mehrmohammadi, M.J. Allen, ACS Omega 2 (2017) 800–805.
- [105] L.A. Basal, M.D. Bailey, J. Romero, M. Meser, L. Ali, J. Kurenbekova, R.G. Yustein, M.J. Pautler, Allen, Chem. Sci. 8 (2017) 8345–8350.
- [106] E. Rodríguez, M. Nilges, R. Weissleder, J.W. Chen, J. Am. Chem. Soc. 132 (2010) 168–177
- [107] A. Bogdanov, L. Matuszewski, C. Bremer, A. Petrovsky, R. Weissleder, Mol. Imaging 1 (2002) 16–23.
- [108] F.A. Cotton, G. Wilkinson, Advanced Inorganic Chemistry, 5 ed., John Wiley & Sons, New York, 1988.
- [109] C. Tu, R. Nagao, A.Y. Louie, Angew. Chem. Int. Ed. 48 (2009) 6547-6551.
- [110] M. Harris, J.L. Kolanowski, E.S. O'Neill, C. Henoumont, S. Laurent, T.N. Parac-Vogt, E.J. New, Chem. Commun. 54 (2018) 12986–12989.
- [111] M. Yu, R.J. Beyers, J.D. Gorden, J.N. Cross, C.R. Goldsmith, Inorg. Chem. 51 (2012) 9153–9155.
- [112] I. Kenkel, A. Franke, M. Dürr, A. Zahl, C. Dücker-Benfer, J. Langer, M.R. Filipović, M. Yu, R. Puchta, S.R. Fiedler, M.P. Shores, C.R. Goldsmith, I. Ivanović-Burmazović, J. Am. Chem. Soc. 139 (2017) 1472–1484.
- [113] M. Yu, S.L. Ambrose, Z.L. Whaley, S. Fan, J.D. Gorden, R.J. Beyers, D.D. Schwartz, C.R. Goldsmith, J. Am. Chem. Soc. 136 (2014) 12836–12839.
- [114] L. Senft, J.L. Moore, A. Franke, K.R. Fisher, A. Scheitler, A. Zahl, R. Puchta, D. Fehn, S. Ison, S. Sader, I. Ivanović-Burmazović, C.R. Goldsmith, Chem. Sci. 12 (2021) 10483–10500.
- [115] M. Yu, M.B. Ward, A. Franke, S.L. Ambrose, Z.L. Whaley, T.M. Bradford, J. D. Gorden, R.J. Beyers, R.C. Cattley, I. Ivanović-Burmazović, D.D. Schwartz, C. R. Goldsmith, Inorg. Chem. 56 (2017) 2812–2826.

- [116] T.E. Hutchinson, A. Bashir, M. Yu, R.J. Beyers, C.R. Goldsmith, Inorg. Chim. Acta 496 (2019) 119045.
- [117] S. Karbalaei, E. Knecht, A. Franke, A. Zahl, A.C. Saunders, P.R. Pokkuluri, R. J. Beyers, I. Ivanović-Burmazović, C.R. Goldsmith, Inorg. Chem. 60 (2021) 8368–8379.
- [118] K. Srivastava, E.A. Weitz, K.L. Peterson, M. Marjańska, V.C. Pierre, Inorg. Chem. 56 (2017) 1546–1557.
- [119] K. Srivastava, G. Ferrauto, V.G. Young, S. Aime, V.C. Pierre, Inorg. Chem. 56 (2017) 12206–12213.
- [120] M.S. Fox, J.M. Gaudet, P.J. Foster, Magn. Reson. Insights 8 (2016) 53-67.
- [121] J. Blahut, L. Benda, J. Kotek, G. Pintacuda, P. Hermann, Inorg. Chem. 59 (2020) 10071–10082.
- [122] R.T. Kadakia, D. Xie, H. Guo, B. Bouley, M. Yu, E.L. Que, Dalton Trans. 49 (2020) 16419–16424.
- [123] R.T. Kadakia, D. Xie, D. Martinez, M. Yu, E.L. Que, Chem. Commun. 55 (2019) 8860–8863.
- [124] J.S. Enriquez, M. Yu, B.S. Bouley, D. Xie, E.L. Que, Dalton Trans. 47 (2018) 15024–15030.
- [125] M. Yu, D. Xie, K.P. Phan, J.S. Enriquez, J.J. Luci, E.L. Que, Chem. Commun. 52 (2016) 13885–13888.
- [126] M. Yu, B.S. Bouley, D. Xie, J.S. Enriquez, E.L. Que, J. Am. Chem. Soc. 140 (2018) 10546–10552.
- [127] K. Wieghardt, U. Bossek, P. Chaudhuri, W. Herrmann, B.C. Menke, J. Weiss, Inorg. Chem. 21 (1982) 4308–4314.
- [128] V.V. Novikov, A.A. Pavlov, Y.V. Nelyubina, M.-E. Boulon, O.A. Varzatskii, Y. Z. Voloshin, R.E.P. Winpenny, J. Am. Chem. Soc. 137 (2015) 9792–9795.
- [129] S. Gomez-Coca, E. Cremades, N. Aliaga-Alcalde, E. Ruiz, J. Am. Chem. Soc. 135 (2013) 7010–7018.
- [130] P.B. Tsitovich, J.M. Cox, J.B. Benedict, J.R. Morrow, Inorg. Chem. 55 (2016) 700–716.
- [131] S.J. Ratnakar, S. Viswanathan, Z. Kovacs, A.K. Jindal, K.N. Green, A.D. Sherry, J. Am. Chem. Soc. 134 (2012) 5798–5800.
- [132] S.J. Ratnakar, T.C. Soesbe, L.L. Lumata, Q.N. Do, S. Viswanathan, C.-Y. Lin, A. D. Sherry, Z. Kovacs, J. Am. Chem. Soc. 135 (2013) 14904–14907.
- [133] P.B. Tsitovich, J.A. Spernyak, J.R. Morrow, Angew. Chem. Int. Ed. 52 (2013) 13997–14000.
- [134] A.M. Funk, V. Clavijo Jordan, A.D. Sherry, S.J. Ratnakar, Z. Kovacs, Angew. Chem. Int. Ed. 55 (2016) 5024–5027.
- [135] K. Du, E.A. Waters, T.D. Harris, Chem. Sci. 8 (2017) 4424–4430.
- [136] G. Liu, Y. Li, M.D. Pagel, Magn. Reson. Med. 58 (2007) 1249-1256.
- [137] B. Song, Y. Wu, M. Yu, P. Zhao, C. Zhou, G.E. Kiefer, A.D. Sherry, Dalton Trans. 42 (2013) 8066–8069.